Although undocumented, Eq. (5) (including this time-dependent term) was used in all published "low-frequency" LTRAN2 calculations by Ballhaus and Goorjian.[1] Also, in the calculations presented here, Eq. (5) will be used by both LTRAN2 and LTRAN2-HI.

Calculated Results and Discussion

Linear Calculations

Computed results from LTRAN2 and LTRAN2-HI are first compared with exact linear theory results. This test serves to establish the capability of the modified code to provide accurate unsteady solutions in the linear domain. The linear theory results are solutions to the "all-frequency" unsteady, transonic small-disturbance equation (i.e., the governing equation includes a ϕ_{tt} term that is neglected in the LTRAN2, LTRAN2-HI codes). Figure 1 displays lift and moment coefficients vs reduced frequency for the case published in Ref. 2 (flat plate pitching 0.25 deg about quarter chord, $\alpha_0 = 0$ deg, $M_\infty = 0.7$). Note that the original LTRAN2 provides reasonably accurate results but only for reduced frequencies less than 0.2. With the exception of the real component of the moment coefficient, LTRAN2-HI gives a more accurate prediction of both lifts and moments over the entire range of reduced frequencies tested. The discrepancy seen in the moment comparison may be attributed to the omission of the ϕ_{tt} term in the governing equation of the codes. Results from Bland[6] verify that calculations from a LTRAN2-HI-type code compare more favorably, almost precisely, with a linear theory formulation also neglecting ϕ_{tt}. Owing to the relatively small magnitude of the real component of moment, LTRAN2-HI still provides the better agreement with linear theory moments in amplitude and phase.[7]

Nonlinear Experimental Comparisons

As stated previously, comparisons with experimental data[5] for a pitching (1 deg about quarter chord) NACA 64A010 airfoil were made at a transonic Mach number of 0.8. Figure 2 displays first harmonic comparisons of lift and moment coefficients vs reduced frequency. The high-frequency modification, in general, produces an improvement in the calculation of real and imaginary components of both lift and moment coefficients over the entire reduced frequency range. The greatest improvement is seen in the determination of the imaginary components where LTRAN2-HI, unlike the original code, captures the experimentally observed trends. Note in particular the successful prediction by LTRAN2-HI of the zero crossing in the imaginary component of the leading-edge moment corresponding to a critical transition from a phase lead to a phase lag. For these reasons, LTRAN2-HI is the recommended version of the code for use in transonic calculations.

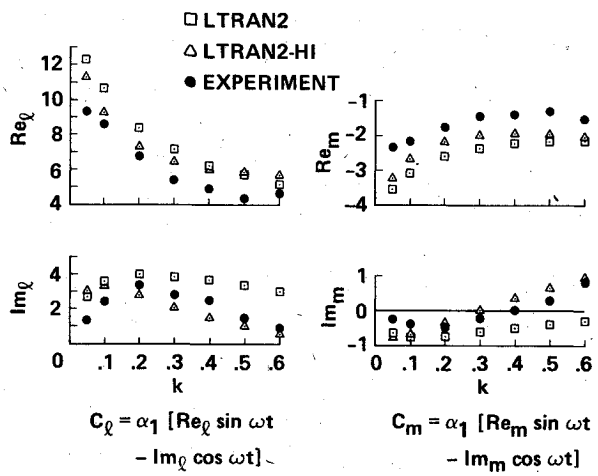

Fig. 2 Lift and leading-edge moment coefficients vs reduced frequency for a pitching NACA 64A010 airfoil, $M_\infty = 0.8$, $k = \omega c/U_\infty$, $\alpha = \alpha_0 + \alpha_1 \sin \omega t$.

The details of these calculations, the algorithmic developments for the modified boundary conditions, as well as additional comparisons with experimental results (unsteady surface pressures for the range of reduced frequencies given in Fig. 2) may be examined in Ref. 7.

Conclusions

LTRAN2-HI, a high-frequency extension of the NASA Ames unsteady, small-disturbance code LTRAN2, provides more accurate unsteady results, as evidenced by experimental comparisons. The modified code is a versatile tool capable of performing reasonably accurate inviscid calculations in both linear and nonlinear flow regimes. Results from the improved code may be obtained at no extra computational expense. LTRAN2-HI has now become the default option of the NASA Ames code LTRAN2.

Acknowledgments

The authors wish to thank S. S. Davis for supplying the linear theory results, as well as W. J. McCroskey and G. N. Malcolm for their comments and suggestions while reviewing the manuscript.

References

[1] Ballhaus, W. F. and Goorjian, P. M., "Implicit Finite Difference Computations of Unsteady Transonic Flows about Airfoils, Including the Treatment of Irregular Shock Wave Motions," *AIAA Journal*, Vol. 15, Dec. 1977, pp. 1728-1735.

[2] Houwink, R. and van der Vooren, J., "Improved Version of LTRAN2 for Unsteady Transonic Flow Computations," *AIAA Journal*, Vol. 18, Aug. 1980, pp. 1008-1010.

[3] Couston, M. and Angelini, J. J., "Numerical Solutions of Nonsteady Two-Dimensional Transonic Flows," *Journal of Fluids Engineering*, Vol. 101, Sept. 1979, pp. 341-347.

[4] Rizzetta, D.P. and Yoshihara, H., "Computations of the Pitching Oscillation of a NACA 64A-010 Airfoil in the Small Disturbance Limit," AIAA Paper 80-0128, Jan. 1980.

[5] Davis, S. S. and Malcolm, G. N., "Experimental Unsteady Aerodynamics of Conventional and Supercritical Airfoils," NASA TM-81221, Aug. 1980.

[6] Bland, S., private communication, NASA Langley Research Center, 1981.

[7] Hessenius, K. A. and Goorjian, P. M., "A Validation of LTRAN2 with High Frequency Extensions by Comparisons with Experimental Measurements of Unsteady Transonic Flows," NASA TM-81307, July 1981.

AIAA 82-4123

A Hybrid Shear Panel

Wayne V. Nack*
Embry-Riddle Aeronautical University
Daytona Beach, Fla.

Introduction

SHEAR panels are used on airframe structures to model thin sheet metal that is attached to heavy stiffeners. The axial load is carried by the stiffeners, which are represented as rods. It is assumed that the sheet metal carries shear stresses at

Received June 15, 1981; revision received Oct. 5, 1981.

*Associate Professor, Department of Aeronautical Engineering. Member AIAA.

the attachment to the stiffener. The sheet metal is then modeled as a shear panel. This Note is not supportive of the modeling procedure, but is intended as a modern update to the shear panel.

The shear panel used in the NASTRAN 1 program was taken from Ref. 2 and is based on the force method. For highly distorted quadrilaterals, the assumptions made in deriving this element are incorrect. Moreover, interelement compatibility is not assured with this panel. A more modern shear panel, based on an equilibrium finite element model, is listed in Ref. 3. A hybrid shear wall was developed in Ref. 4 to model building walls connected to beam columns and rigid floors. This shear wall requires two translational and one rotational degrees of freedom at each node.

The rectangular hybrid element of Refs. 5 and 6 will be specialized for a shear panel by finding an internal stress distribution that produces only shear stresses on the element boundaries. This element is compatible on interelement boundaries and can be integrated with a finite element program.

Internal Stresses

The Airy stress function was used in polynomial form to find biharmonic functions which satisfy

$$F_{xxxx}+2F_{xxyy}+F_{yyyy}=0$$

The function F contained a combination of polynomials given in the Pascal triangle of Ref. 6. Rows 3-8 of the Pascal triangle were used for the stress function and to satisfy the biharmonic equation; certain dependencies were found between some of the coefficients. A total of twenty linearly independent functions were found that satisfied the biharmonic equation. The twentieth function was a combination of two asymmetric solutions that produced a symmetric polynomial. The stresses were recovered from the stress function by

$$S_x=F_{yy},\quad S_y=F_{xx},\quad S_{xy}=-F_{xy}$$

The stresses depended on twenty unknown coefficients.

On the boundary of a quadrilateral element it is assumed that the normal stress vanishes and the shear stress is constant on each side. By statics, the set of shear stresses can be expressed in terms of one unknown shear stress b and a set of coefficients that depend only on the geometry. The normal and shearing stresses at a boundary are found from the stress transformation

$$S_N=S_x\cos^2\theta+S_y\sin^2\theta+S_{xy}\sin 2\theta$$

$$\tau_N=-[(S_x-S_y)/2]\sin 2\theta+S_{xy}\cos 2\theta$$

The twenty unknown constants can all be expressed in terms of one unknown shear stress b. To determine these constants, the normal stress was set to zero at the quarter and three-quarter point of each side, and the shear stresses were set to the values in terms of b at the eighth, half, and seven-eighths point of each side.

For a rectangular panel, the stress distribution found was constant shear and for a parallelogram, a constant normal and shear stress resulted. It was found that at least twenty terms were needed in the Airy stress function for sufficient accuracy.

Hybrid Shear Panel

The modified complementary energy[7,8] was used to derive the shear panel. If the stresses are an equilibrium field and if the loading results from concentrated loads at the node points, this variational statement minimizes the following:

$$\pi^*=U^*(\sigma)-\int_S \bar{u}^T t\,ds$$

where $U^*(\sigma)$ is the complementary energy, $\delta U^*(\sigma)=\int_V \delta\sigma\epsilon$, $\bar{u}$ are displacements, t are tractions, V is the volume, S the boundary surface, σ the stresses, and ϵ the strains.

In the hybrid element formulation, displacements are interpolated on the element boundary, while stresses are interpolated in the interior. The stresses are found in terms of one unknown shear stress b from the polynomial representation and the point collocation on the boundary. The 3×1 stress, matrix, in terms of the scalar b, is $\sigma=Nb$. The strain stress relation for plane stress is $\epsilon=C\sigma$.

To interpolate the displacements, a linear function is assumed between the end points, A,B of one side,

$$q=q_A[1-(s/L)]+q_B(s/L)$$

The parameter s is measured from point A to B along the side, and L is the length of the side AB.

The 8×1 matrix of displacements is given by

$$\bar{u}=\bar{N}a,\quad a=(u_1v_1\cdots u_4v_4)^T$$

$\bar{N}=8\times 8$ matrix of displacement interpolants

The X-Y components of tractions on each side are given by

$$t=G\sigma$$

The G_s matrix for one side is

$$G_s=\begin{vmatrix} n_x & 0 & n_y \\ 0 & n_y & n_x \end{vmatrix}$$

where n_x, n_y are direction cosines of the outward normal to that side

$$n_x=\frac{Y_A-Y_B}{L},\quad n_y=\frac{X_B-X_A}{L}$$

The G_s matrix is repeated for each side to form the G matrix of 8×3 size with the traction freedoms (rows) in the same order as the displacement freedoms. In terms of these matrices, the modified complementary energy is

$$\pi^*=\tfrac{1}{2}b^THb-a^TPb,\quad H=\int N^TCN t\,dx\,dy,\quad P=\int_S \bar{N}^TGN\,dS$$

The H scalar is numerically integrated by transforming to isoparametric coordinates using a bilinear transform of corner nodes. The limits on P correspond to the length of the side being calculated, and numerical integration is used.

The shear stress b is independent of other elements. It is eliminated as a nodeless variable. The stationary requirement of π^* is

$$\frac{\partial\pi^*}{\partial b}=0=Hb-P^Ta$$

$$b=H^{-1}P^Ta$$

$$\frac{\partial\pi^*}{\partial a}=-Pb=-PH^{-1}P^Ta$$

The stiffness matrix is identified as $K=-PH^{-1}P^T$.

Numerical Results

Figure 1 shows a three-cell cantilever beam composed of three rectangular shear panels and ten rods derived by the displacement method. The geometry and material properties are also shown in the figure. The tip deflection of a cantilever including shear deformation is

$$\delta=PL^3/3EI+PL/Ght$$

The calculated deflection was 0.1956 mm by the formula, which agreed with the hybrid panel tip deflection at 0.1943 mm. By the formula, the deflection was 34% due to shear, which checked the deflection characteristics of the panel.

Figure 2 shows a system of shear panels and rods that is internally redundant on the four cells. The classical force transfer solution given in Ref. 9 is shown and compared to the hybrid method in the figure. A displacement incompatibility between the large element on the left and the four cells was introduced in the hybrid method.

It should be noted that the load transfer mechanism used by the hybrid method is different from the classical force transfer approach of Ref. 9. The hybrid method has a constant force in each rod, while the force approach assumes a linearly varying force. However, there was fairly good agreement between the two methods in the shear flows shown in Fig. 2. This panel could be extended to include a linear varying force in each rod that would be analogous to Ref. 9.

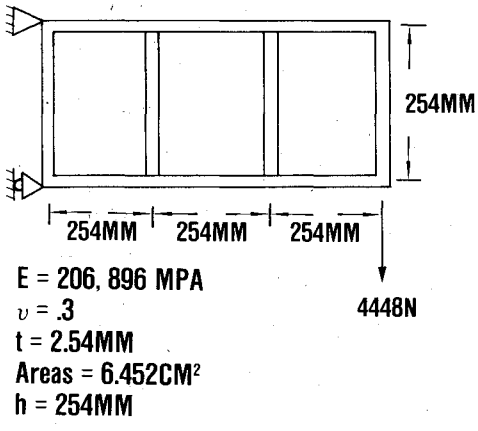

Fig. 1 Shear panel cantilever.

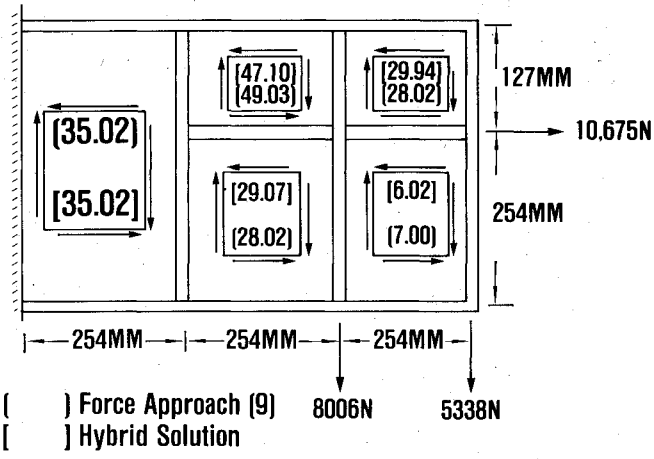

Fig. 2 Shear flows, N/mm².

Conclusion

The hybrid shear panel takes a constant shear stress along each edge with no normal stress. The panel is compatible only along interelement boundaries and is not compatible within the element. The panel may be distorted into a quadrilateral, although no numerical results could be found in the literature for comparison. Equilibrium is forced at the node points and is not assured everywhere, although the shear stresses along each panel are in equilibrium with the panel.

This panel could be extended to include warpage effects, and extensions could be made to integrate the panel with linear force varying rods to improve the equilibrium characteristics.

References

[1] MacNeal, R. H., *The NASTRAN Theoretical Manual,* NASA SP-221, 1976.

[2] Garvey, S. J., "The Quadrilateral Shear Panel," *Aircraft Engineering,* May 1951, pp. 134-135.

[3] Robinson, J., "A Six Node Triangular Shear Panel for Equilibrium Models," *RA/ARD,* Rept. No. 25-4-73-14, April 1973.

[4] Kabaila, A. P. and Edwards, R. J., "Hybrid Element Applied to a Shear Wall Analysis," *Journal of Structural Division,* Vol. 105, Dec. 1979.

[5] Cook, R. D. and Al-Abdulla, J. K., "Some Plane Quadrilateral Hybrid Finite Elements," *AIAA Journal,* Vol. 7, Nov. 1979, pp. 2184-2185.

[6] Zienkiewicz, O. C., *The Finite Element Method,* 3rd ed., McGraw-Hill, New York, 1977, pp. 304-325.

[7] Washizu, K., *Variational Methods in Elasticity and Plasticity,* Pergamon Press, New York, 1975, pp. 8-38.

[8] Gallagher, R. H., *Finite Element Analysis Fundamentals,* Prentice-Hall, New Jersey, 1975, pp. 135-210.

[9] Peery, D. J., *Aircraft Structures,* McGraw-Hill, New York, 1950, pp. 181-195.

AIAA 82-4124

Time-Dependent Adhesive Behavior Effects in a Stepped Lap Joint

M. M. Ratwani,* H. P. Kan,† and D. D. Liu‡
Northrop Corporation, Hawthorne, Calif.

Introduction

INCREASING use of adhesive bonding in aerospace structures requires that analysis methods be available in the areas of service life and strength predictions. Adhesives exhibit viscoelastic (time-dependent) behavior, i.e., the stress-strain relation is a function of time. This behavior will influence stress distribution in adhesively bonded structures. Also, any life prediction technique will be influenced by the viscoelastic behavior of adhesives. Hence, the time-dependent behavior of adhesively bonded structures must be properly understood.

An extensive study of time-dependent behavior of adhesively bonded joints has been carried out by Romanko and Knauss.[1] The method of modeling viscoelastic behavior, based on experimental observations, is also discussed in Ref. 1. For rigid adherends, the influence of time-dependent adhesive behavior on a metal-to-metal bonded joint has been investigated in this reference, and the stress distribution is shown to be time-independent. In reality the adherends are never rigid, and the influence of elastic behavior of adherends should be taken into consideration. The analytical techniques developed by Erdogan and Ratwani[2] for elastic adherends are extended to take into consideration the time-dependent behavior of the adhesives.

Viscoelastic Model for Adhesive Behavior

The viscoelastic behavior of typical structural adhesives (such as epoxy adhesives FM73 and FM400[1]) can be

Received Jan. 14, 1980; revision received Sept. 14, 1981.

†Engineering Specialist, Structural Life Assurance Research. Member AIAA.

‡Engineering Specialist, Structural Dynamics Research. Member AIAA.